NANO LETTERS
Letter
Cite This: Nano Lett. 2019, 19, 8021−8031
pubs.acs.org/NanoLett

Combretastatin A4 Nanoparticles Combined with Hypoxia-Sensitive Imiquimod: A New Paradigm for the Modulation of Host Immunological Responses during Cancer Treatment

Na Shen,[†,§,#] Jing Wu,[‡,§,#] Chenguang Yang,[†,§] Haiyang Yu,[†,§] Shengcai Yang,[†,§] Tete Li,[‡] Jingtao Chen,[*,‡] Zhaohui Tang,[*,†,§] and Xuesi Chen[*,†,§]

[†]Key Laboratory of Polymer Ecomaterials, Changchun Institute of Applied Chemistry, Chinese Academy of Sciences, Changchun 130022, PR China

[‡]Institute of Translational Medicine, The First Hospital of Jilin University, Changchun 130022, PR China

[§]Jilin Biomedical Polymers Engineering Laboratory, Changchun 130022, PR China

Supporting Information

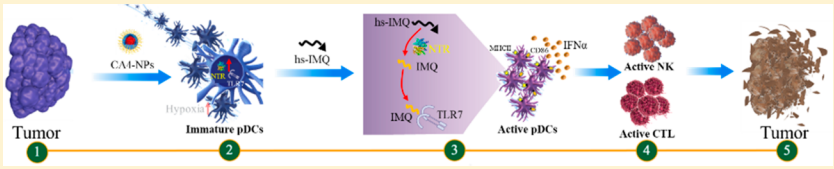

ABSTRACT: Vascular disrupting agents (VDAs) have great potential in cancer treatment. However, in addition to their direct tumoral vascular collapse effect, VDAs activate host immunological responses, which can remarkably impair their anticancer efficacy. Here, a VDA nanomedicine, poly(L-glutamic acid)-*graft*-methoxy poly(ethylene glycol)/combretastatin A4 (CA4-NPs), is found to induce the intratumor infiltration of immature plasmacytoid dendritic cells (pDCs), thereby curtailing anticancer immunity. To overcome this problem, hypoxia-sensitive imiquimod (hs-IMQ) is developed, which is selectively activated into imiquimod (IMQ) in treated tumors following the catalysis of CA4-NPs-induced nitroreductase (NTR). The combination of hs-IMQ and CA4-NPs causes a 6.3-fold enhancement of active IMQ concentration in tumors, as compared to hs-IMQ treatment alone. The *in situ*-generated IMQ alters the tumor microenvironment from a state of immunosuppression to immune activation. Hs-IMQ achieves this effect through the conversion of immature pDCs into their active form, leading to the robust infiltration and priming of natural killer cells and cytotoxic T-lymphocytes in treated tumors. Thus, the CA4-NPs and hs-IMQ combination treatment synergistically inhibits tumor growth and metastasis in 4T1 tumor-bearing mice. This work offers new approaches to harness intratumor pDCs to reverse the immune suppression resulting from VDA treatment. These findings additionally provide a mechanistic rationale for the use of VDAs in combination with TLR agonists to trigger *in situ* immune activation and enhance anticancer efficacy.

KEYWORDS: *Nanomedicines, vascular disrupting agents, drug delivery, hypoxia-sensitive, tumor immunotherapy*

The immune system influences cancer formation, development, and progression, through both host-protective (elimination) and tumor-promoting (escape) roles.[1−3] The host immunological responses to anticancer therapy have a pivotal influence on the therapeutic outcome[4−6] and can be used to predict patient prognosis.[7−11] In particular, the host immunological response is an essential contributor to drug resistance[5,12−15] and can induce a loss of drug-responsiveness and subsequent tumor regrowth and/or relapse.[12,16−19] Since the host immunological "side" effects of cancer therapy are undesirable, gaining an in-depth understanding of their underlying mechanisms facilitates the design of novel combinatorial regimens with improved clinical efficacy.[20−22]

The tumor vasculature represents a key target in cancer therapy due to its critical role in the survival and growth of solid tumors. Accordingly, vascular disrupting agents (VDAs) have great therapeutic potential through their ability to selectively destroy the vasculature of solid tumors, resulting in extensive tumor necrosis. Several small molecule VDAs are under investigation in clinical trials,[23,24] but tumor regrowth is frequent,[25−27] compromising the efficiency of VDA therapy.[25,26,28] TIE2$^+$ tumor-associated macrophages (MΦ) and endothelial progenitor cells infiltrate tumors after treatment with small-molecule VDAs such as combretastatin A4 phosphate (CA4P) and OXi-4503, promoting tumor angiogenesis, outgrowth, and relapse, despite an initial successful therapeutic outcome.[29−31] This indicates that the host immunological response plays an important role in the failure of VDA treatment. Further studies in this area will enrich this knowledge and provide new insights into VDA-based tumor resistance.

Received: August 5, 2019
Revised: September 20, 2019
Published: September 27, 2019

DOI: 10.1021/acs.nanolett.9b03214
Nano Lett. 2019, 19, 8021−8031

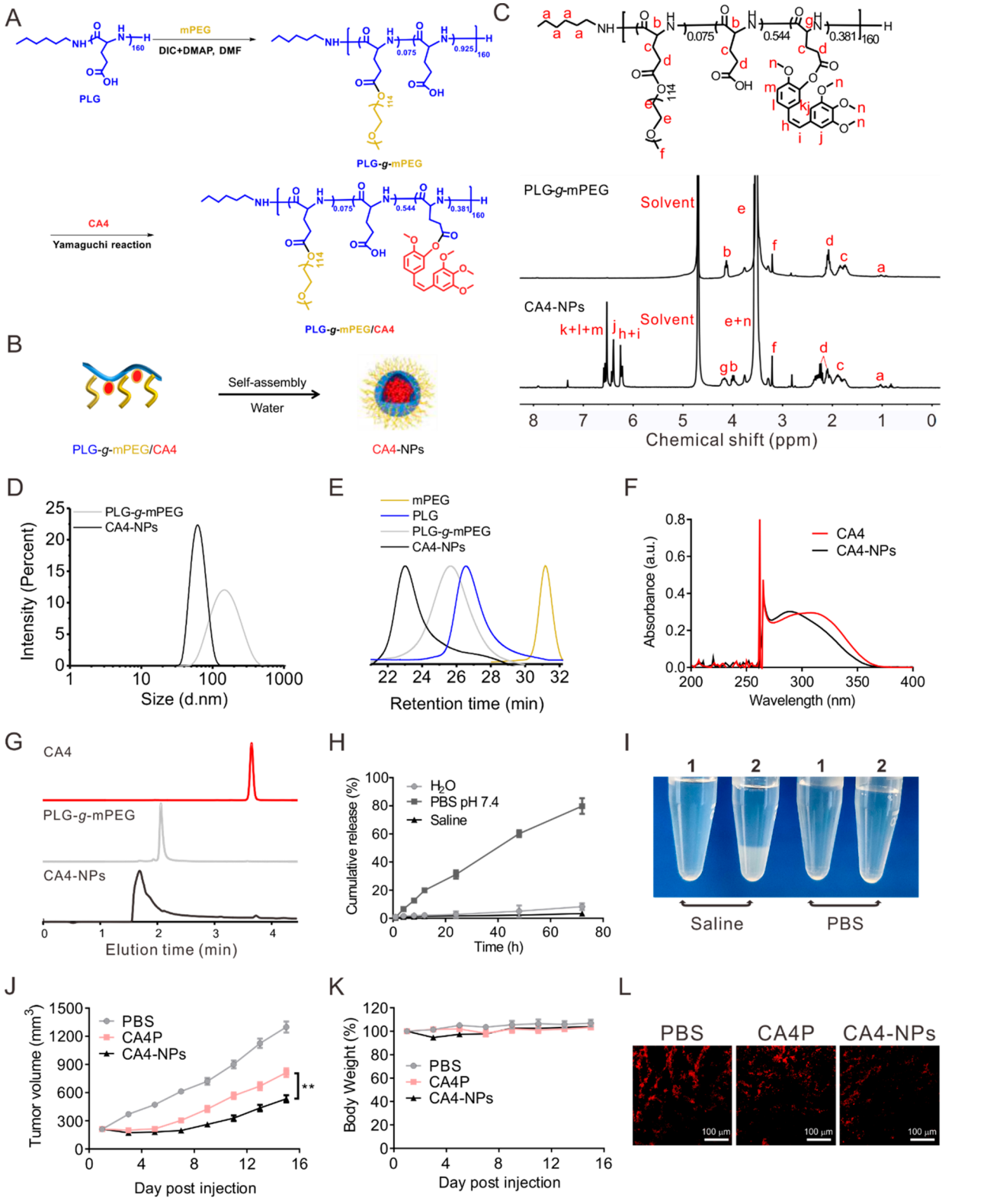

Figure 1. Preparation and characterization of CA4-NPs. (A) Synthesis process of PLG-*g*-mPEG/CA4. (B) Schematic image for preparation of CA4-NPs. (C) ^{1}H NMR spectra of PLG-*g*-mPEG and CA4-NPs in NaOD/D_2O. (D) DLS analyses of PLG-*g*-mPEG and CA4-NPs in deionized water. (E) GPC curves of mPEG, PLG, PLG-*g*-mPEG, and CA4-NPs. (F) UV−vis spectra of CA4 and CA4-NPs in DMF. (G) HPLC curves of CA4, PLG-*g*-mPEG, and CA4-NPs. Monitoring was performed with a UV detector at 289 nm. (H) Cumulative CA4 release of CA4-NPs in different conditions, including water, 0.01 M PBS pH 7.4, and physiological saline. (I) Water solubility of CA4-NPs (1) and PLG-CA4 (2). CA4-NPs or PLG-CA4 was dissolved with physiological saline or 0.01 M PBS pH 7.4 at a concentration of 1.0 mg/mL (on the CA4 basis). The picture was taken 30 min after solvent was added to the drugs. (J, K) 4T1 tumor growth curve (J) and body weight change (K) after CA4P or CA4-NPs (45 mg/kg equiv to CA4, iv injection at Day 1 treatment. (L) CD31 staining for CA4P or CA4-NP-treated tumors.

DOI: 10.1021/acs.nanolett.9b03214
Nano Lett. 2019, 19, 8021−8031

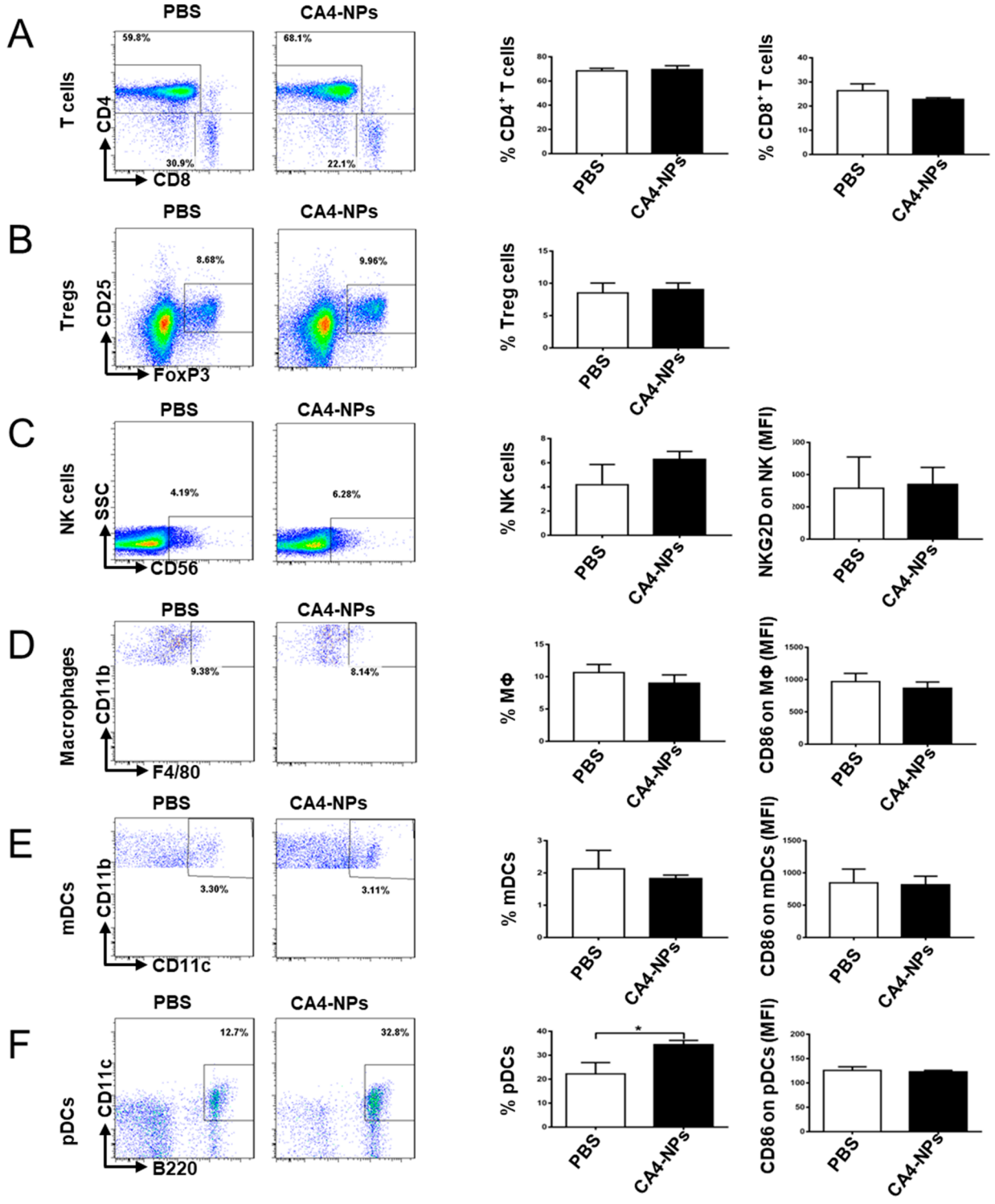

Figure 2. Host immunological responses 5 days post-treatment. The 4T1 tumor-bearing mice were injected with CA4-NPs (45 mg/kg equiv to CA4) or PBS via the tail vein. (A–F) Intratumoral $CD4^+$ T cells/$CD3^+$ T cells (A, left panel), $CD8^+$ T cells/$CD3^+$ T cells (A, right panel), Treg cells/$CD4^+$ T cells (B), NK cells/$CD45^+$ cells and NKG2D on NK cells (C), macrophages/$CD3^-CD19^-$ cells and CD86 on macrophages (D), mDCs/$CD3^-CD19^-$ cells and CD86 on mDCs (E), pDCs/$CD3^-CD19^-$ cells and CD86 on pDCs (F) were analyzed by flow cytometry. The levels of the indicated activation markers were expressed as the mean fluorescence intensity (MFI). Data are shown as the mean ± SEM. Representative data from one of three independent experiments are shown. Paired *t* tests were used for all statistical comparisons (*$p < 0.05$).

Combretastatin A4 (CA4) is a lead agent in VDAs. However, because of its poor aqueous solubility, CA4 cannot directly be intravenously administrated. Although many small-molecule prodrugs of CA4 have been developed to improve its solubility, the overall therapeutic efficiency is moderate.[32] A key reason for this is the reversible effect that CA4 has on tubulin as well as its rapid clearance from plasma and tissues.[32] As CA4 is difficult to directly encapsulate and CA4P is water-soluble, we previously designed a covalent bonding CA4 nanodrug (PLG-CA4) that exhibited high distribution and

DOI: 10.1021/acs.nanolett.9b03214
Nano Lett. 2019, 19, 8021–8031

gradual release around tumor blood vessels, resulting in prolonged vascular disruption and markedly enhanced therapeutic efficiency compared to CA4P.[32] However, the solubility of PLG-CA4 in saline is still poor. In this study, we assessed CA4-NPs with a higher mPEG content than the PLG-CA4 to improve solubility. We further investigated the host immunological response after CA4-NPs treatment in metastatic 4T1 breast carcinoma model. The host immunological side effects were converted to a selective treatment advantage using the combined regimen of CA4-NPs and a novel hypoxia-sensitive imiquimod.

The nanoparticle preparation was shown in Figure 1A,B. The ^{1}H NMR spectrum (300 M, NaOD/D_2O) of CA4-NPs was shown in Figure 1C. Typical peaks in the ^{1}H NMR spectrum at δ 6.53 (k + l + m), 6.41 (j), and 6.26 (h + i) ppm should be assigned to the protons of CA4 in the CA4-NPs. Thirty-eight percent of glutamic acid moieties was conjugated with CA4. The CA4-NPs had a hydrated size of 72.5 ± 2.5 nm, smaller than poly(L-glutamic acid)-*graft*-methoxy poly(ethylene glycol) (PLG-*g*-mPEG, 148.5 ± 10.3 nm) (Figure 1D). In view of the composition of PLG-*g*-mPEG, the side groups in deionized water would exist in the format of −COOH, making the PLG moiety hydrophobic, so PLG-*g*-mPEG tended to form relatively unstable micelles, while the micelles became more compact after CA4 was covalently bonded. The M_n and M_w/M_n of CA4-NPs determined by GPC were 114 kDa and 1.20, respectively. The GPC spectra showed that the average molecular weight varied as PLG-*g*-mPEG/CA4 (CA4-NPs) > PLG-*g*-mPEG > PLG (Figure 1E), indicating that mPEG and CA4 were successfully conjugated to the PLG. UV−vis spectra indicated that the wavelength of the CA4 maximum absorbance had a red shift after grafting to PLG-*g*-mPEG. The CA4-NPs in DMF showed an absorption peak at 289 nm in the UV−vis spectrum, while CA4 had an absorption peak at 308 nm (Figure 1F). As shown in Figure 1G, the CA4-NPs showed only modest free CA4 signals in the HPLC curve with UV-detector monitoring at 289 nm, suggesting that the purity of the obtained CA4-NPs exceeded 99%. The release profiles of CA4-NPs were shown in Figure 1H. The CA4-NPs were stable in pure water, while significant CA4 release was observed in PBS pH 7.4, which indicated CA4-NPs could release CA4 in physical pH condition. The accumulative release of CA4-NPs in physical pH condition at 4 h was 6.5 ± 0.49%. Given that the blood circulation of a drug administrated by iv injection was fast, we inferred that CA4-NPs would be the major format of total CA4 that arrived at tumors. Moreover, the water solubility of CA4-NPs was markedly higher than that of PLG-CA4 in physiological saline, indicating the CA4-NPs was more suitable for clinical application (Figure 1I). According to the release and solubility data, we can conclude that CA4-NPs were more stable in physical saline and pure water, as weakly alkaline ion could catalyze the release of CA4 when CA4-NPs were dissolved in PBS pH 7.4. As to the tumor inhibition ability, the therapeutic efficacy of CA4-NPs (45 mg/kg, equiv to CA4) was significantly improved compared to that of CA4P (45 mg/kg, equiv to CA4) without obvious body weight loss (Figure 1J,K). Furthermore, endothelial cells were identified by immunofluorescence labeling of tumor sections using a platelet−endothelial cell adhesion molecule (CD31), which indicated that tumor vessel was reduced to a deeper extent in the CA4-NPs group than in the CA4P group (Figure 1L). Thus, the above synthesized CA4-NPs had accurate structures, appropriate sizes, good solubility properties, and potential anticancer capabilities.

The immune responses of CA4-NPs-treated 4T1 tumors (initial tumor volume 500 mm^3) were analyzed by flow cytometry, including the detection of $CD4^+$ T cells, $CD8^+$ T cells, Treg cells, natural killer (NK) cells, and NKG2D on NK cells, macrophages and CD86 on macrophages, myeloid dendritic cells (mDCs) and CD86 on mDCs, and pDCs and CD86 on pDCs. As shown in Figure 2, pDCs were significantly recruited to the tumors after 5 days of CA4-NPs treatment while other immune cells showed no obvious changes. Recruited pDCs were mainly in the immature form, as the fold increase of the mean fluorescence intensity of CD86 on pDCs (CD86 is a marker of active pDCs) in whole tumors was much lower than that of the pDCs percentage. These indicated that CA4-NPs treatment inducing the intratumor infiltration of immature pDCs.

We further analyzed the factors contributing to the recruitment of pDCs to CA4-NPs-treated tumors. Considerable evidence has emerged that CXCL12/CXCR4 influences pDC tumor migration.[33] CXCL12 is upregulated in hypoxic conditions,[34] and its plasma levels are increased in CA4P-treated patients.[35] The tumor expression of CXCL12 increased 24 h after CA4P treatment.[36] In the present study, the CXCL12 signal was significantly elevated in the tumors of 4T1-bearing Balb/c mice after 5 days of treatment with 45 mg/kg CA4-NPs (equiv to CA4), as determined by enzyme-linked immunosorbent assays (Figure S1). These data suggested that the increased CXCL12 levels accounted for the homing of pDCs to the CA4-NPs-treated tumors.

As one of the major populations of dendritic cells (DCs), pDCs bridge the innate and adaptive immune systems.[37−39] Immature pDCs contribute to the establishment of an immunosuppressive tumor microenvironment by promoting tumor cell growth.[40−42] However, upon activation, pDCs undergo phenotypic changes that result in the upregulation of MHC II[43] and costimulatory molecules including CD40, CD80, and CD86.[44] These active pDCs activate NK cells and mDCs promote the survival, memory, and IFN-γ production of T-cells and induce B-cell differentiation into plasma cells.[45] Clinical studies have demonstrated an inverse correlation between the number of infiltrating pDCs and patient prognosis.[46] Active pDCs can effectively eliminate tumors.[47,48] CA4-NPs treatment led to a significant mobilization of immature pDCs to tumors, potentially explaining its therapeutic efficacy. Thus, the regulation of immature pDCs could potentially improve the therapeutic efficacy of CA4-NPs. To achieve this, the infiltrated immature pDCs in tumors after CA4-NPs treatment should be converted to an active form.

To circumvent the adverse effects of immature pDC infiltration into CA4-NPs-treated tumors, while maintaining *in situ* pDCs, we focused on the Toll-like receptor 7 agonist IMQ, a widely used topical immune response modifier that converts immature pDCs into tumor-killing effector cells.[47,49,50] IMQ is a U.S. Food and Drug Administration-approved drug for external genital warts, actinic keratoses, and superficial basal cell carcinomas. However, IMQ is only locally administered as a cream[51] and is unsuitable for systemic administration due its lack of tumor targeting and side effects.[52−54]

Given the hypoxic status of the tumor microenvironment of VDAs treatment,[55] we synthesized a hypoxia-sensitive derivative of IMQ (hs-IMQ) (Figure 3A and Figure S2) that

DOI: 10.1021/acs.nanolett.9b03214
Nano Lett. 2019, 19, 8021−8031

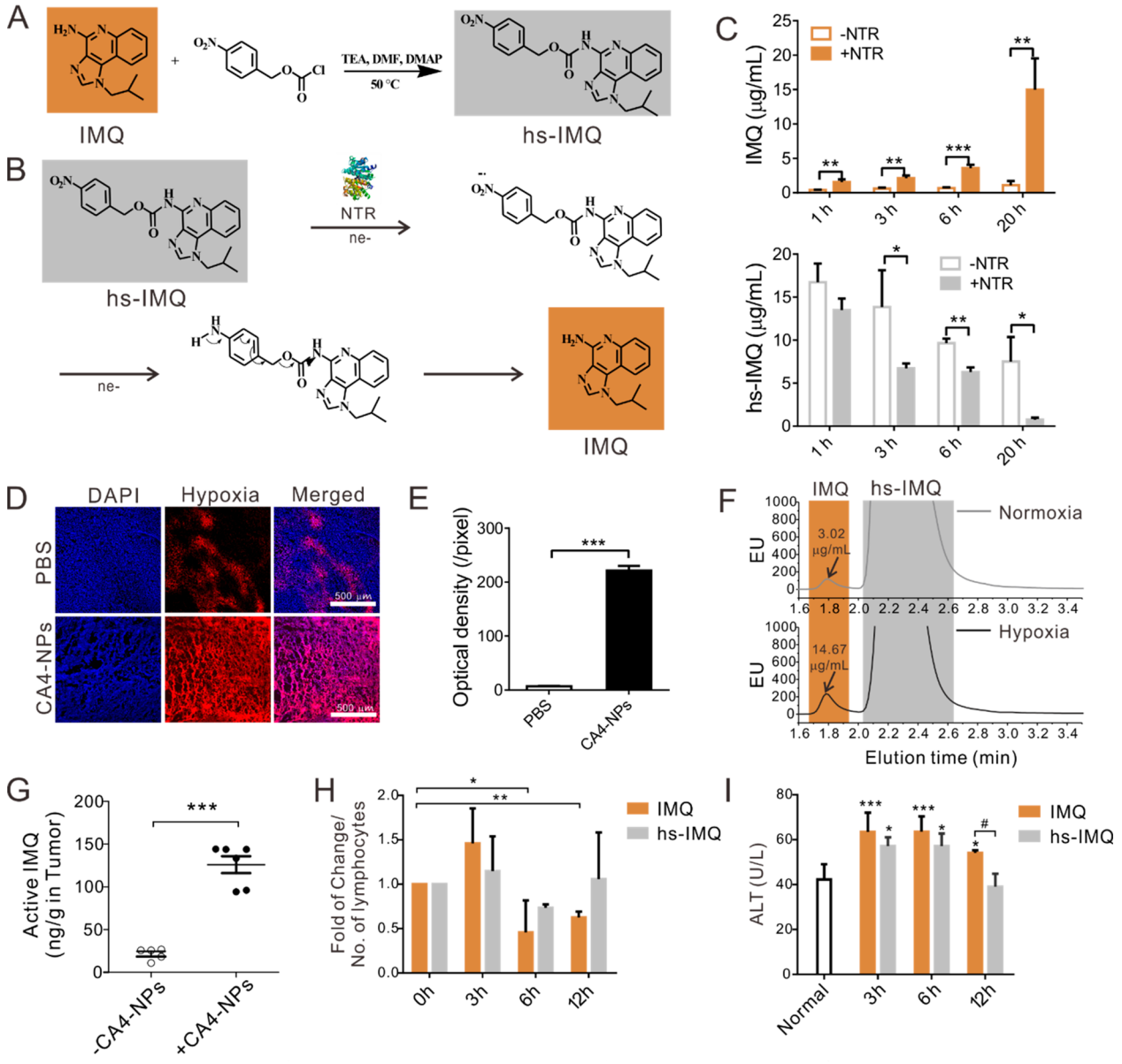

Figure 3. Synthesized hs-IMQ is responsive to nitroreductase (NTR) and CA4-NPs-induced hypoxia. (A, B) Synthesis routes (A) and activation mechanisms (B) of hs-IMQ. (C) IMQ and hs-IMQ concentrations for hs-IMQ release under NTR catalysis (1, 3, 6, and 20 h). (D, E) Confocal microscope images (D) and quantification (E) of hypoxia induction in tumors after CA4-NPs (45 mg/kg equiv to CA4) treatment for 24 h. (F) HPLC analyses for hs-IMQ release *ex vivo* under normoxia or hypoxia. (G) Quantification of active IMQ for drug distribution in tumors subjected to 8 mg/kg hs-IMQ (equiv to IMQ) with 45 mg/kg CA4-NPs (equiv to CA4, $n = 6$ mice/group) or without CA4-NPs ($n = 5$ mice/group). (H, I) Toxicity of IMQ and hs-IMQ in normal rats. Level change of lymphocytes (H, $n = 3$ rats/group) and ALT ($n = 4$ rats/group) level (I) at different times after IMQ (8 mg/kg) and hs-IMQ (8 mg/kg equiv to IMQ) treatment. For (H), each number of lymphocytes at different time points was normalized by its own initial number of lymphocytes (0 h). One-way ANNOVA was used for statistical comparisons ($^*p < 0.05$, $^{**}p < 0.01$). For (I), the average ALT at 0 h was noted as "normal". One-way ANNOVA was used for statistical comparisons ($^*p < 0.05$, $^{**}p < 0.01$, $^{***}p < 0.001$ for different time points) and normal comparison ($^{\#}p < 0.05$ for IMQ and hs-IMQ comparison).

permitted systemic administration. Further, the hs-IMQ derivative could convert intratumor immature pDCs to their active form, thereby enhancing the antitumor efficacy of CA4-NPs treatment. *In vitro* experiments confirmed that hs-IMQ is catalyzed to its active form in the presence of nitroreductase (NTR) (Figure 3B,C). Pimonidazole is a hypoxia probe that forms adducts with thiol-rich macromolecules in a complex series of bioreductive reactions catalyzed by cellular NTR enzymes in hypoxic conditions.[56,57] Pimonidazole also serves as an NTR reporter.[58−60] We coadministered Pimonidazole with 45 mg/kg CA4-NPs to (equiv to CA4)-treated 4T1-bearing Balb/c mice and imaged frozen tumor slices through confocal microscopy. Elevated NTR levels after CA4-NPs treatment were observed, indicating that the tumor microenvironment became markedly hypoxic (Figure 3D,E). In addition, IMQ release in *ex vivo* pDCs and the tumor selectivity of hs-IMQ *in vivo* were assessed. The hs-IMQ was added to pDC culture media under normoxia and hypoxia for 24 h, and free IMQ and hs-IMQ in cells were analyzed by HPLC. The levels of active IMQ were 4.86-fold higher under hypoxia compared to normoxia (Figure 3F). The combination of hs-IMQ and CA4-NPs led to a 6.3-fold increase in the active

DOI: 10.1021/acs.nanolett.9b03214
Nano Lett. 2019, 19, 8021−8031

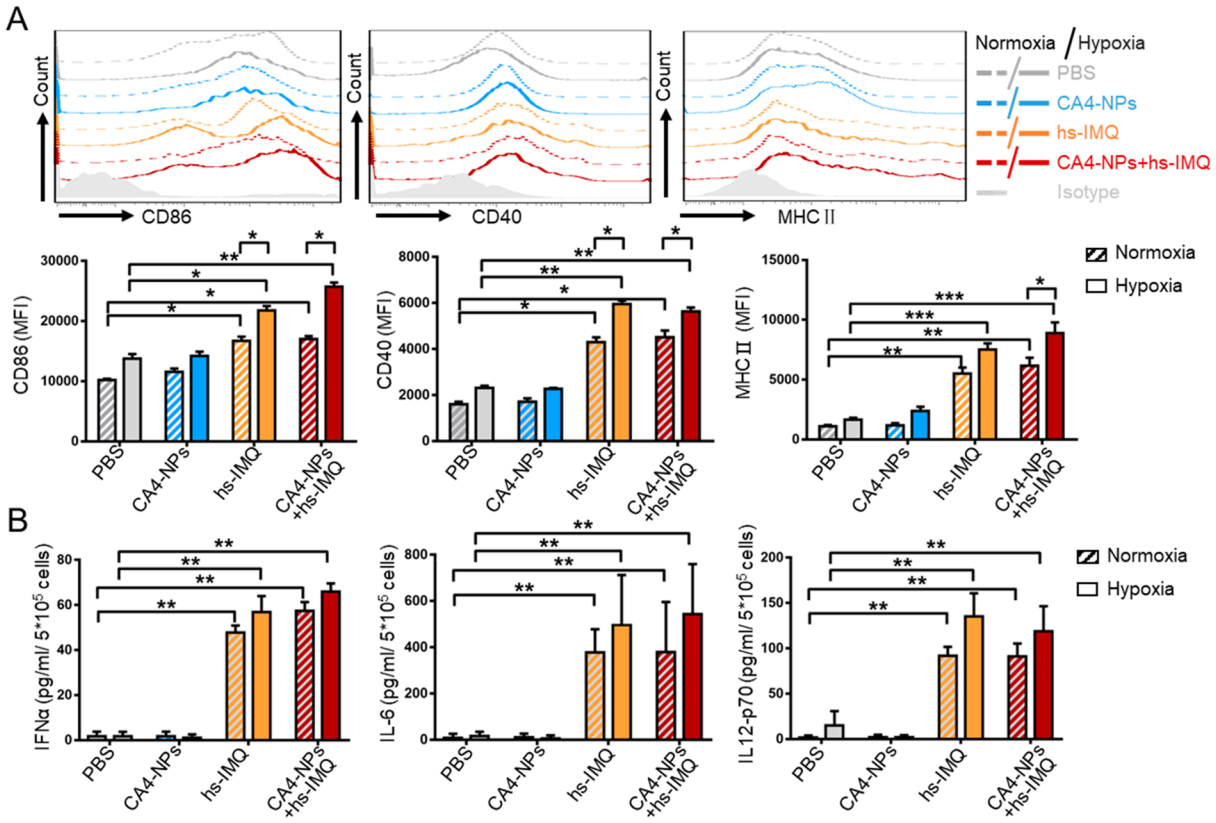

Figure 4. pDC activation by hs-IMQ ex vivo. pDCs (0.5×10^6) were treated with saline, CA4-NPs, hs-IMQ, or CA4-NPs + hs-IMQ under normoxia or hypoxia conditions for 48 h. Hs-IMQ (eq 1 mg/mL IMQ), CA4-NPs (eq CA4: IMQ 15:8). (A) Flow cytometry results reflecting the expression of the indicated activation molecules. (B) ELISA results for the detection of the indicated secreted cytokines. One-way ANNOVA was used for statistical comparisons (*$p < 0.05$, **$p < 0.01$, ***$p < 0.001$).

form of IMQ (Figure 3G). These data demonstrate that hs-IMQ is hypoxia-sensitive and that CA4-NPs-treatment promotes tumor hypoxia.

According to previous reports,[52−54] IMQ can cause lymphopenia and abnormal liver function (including alanine aminotransferase, ALT, a classic inflammation marker of liver function) and other inflammation marker increases. Thus, levels of lymphocytes and ALT were tested in normal 8 week old (180−200 g) female rats after 8 mg/kg IMQ or 8 mg/kg hs-IMQ (equiv to IMQ) i.p. injection after various times during the study. Compared with the 0 h time point, the level of lymphocytes at the 6 and 12 h time points were significantly reduced in the IMQ group, whereas there was no significant change at different time point in the hs-IMQ group, relative to 0 h (Figure 3H). Meanwhile, ALT levels at 3, 6, and 12 h in the IMQ group significantly increased, compared to the ALT level in normal rats, while ALT levels in the hs-IMQ group at the 3 and 6 h time points increased and then were back to the normal level at 12 h. At the 12 h time point, the hs-IMQ group had a significantly lower level of ALT, compared with the IMQ group. The ALT level was numerically higher in the IMQ group than that in hs-IMQ (Figure 3I). Collectively, the systemic toxicity reduced after IMQ was modified to hs-IMQ.

To evaluate the ability of hs-IMQ to activate pDCs, *ex vivo* experiments were performed. The pDCs were extracted from the bone marrow of Balb/c mice and cocultured with CA4-NPs, hs-IMQ, or CA4-NPs + hs-IMQ. Phosphate-buffered saline (PBS) was used as a control. Following activation by hs-IMQ, the cell surface expression of MHC II, CD40, and CD86 on pDCs significantly increased, with greater effects observed under hypoxia (Figure 4A). Accordingly, the pDCs displayed significantly enhanced cytokine secretion including IFNα, IL-6, and IL-12p70 in hypoxic conditions (Figure 4B). These results indicate that hs-IMQ promotes the maturation and activation of pDCs more efficiently in hypoxic conditions.

The *in vivo* antitumor effects of combined hs-IMQ and CA4-NPs were then evaluated in 4T1 tumor-bearing female Balb/c mice. When the tumors reached 200 mm^3, mice were administered PBS, 45 mg/kg CA4-NPs (eq to CA4), 8 mg/kg hs-IMQ (eq to IMQ), or 45 mg/kg CA4-NPs (eq to CA4) + 8 mg/kg hs-IMQ (eq to IMQ) (Figure 5A). Notably, the tumor inhibition rates reached 87% in mice receiving the combination treatment, which were significantly higher than all other groups (Figure 5B). The tumor inhibition efficacy was also compared by H&E staining, which showed a diffuse tumor cell growth without signs of apoptosis or necrosis in untreated tumors (PBS group), most confluent areas of dead cells with typical loss of nuclei could be found in tumor cells of the CA4-NPs + hs-IMQ group (Figure S3). Moreover, no significant change in body weight occurred during the treatment period (Figure 5C) and the histological staining showed that all the treatments did not have obvious toxicity to tissues like heart, spleen, and kidney (Figure S4). As expected, India ink assays showed that lung metastasis was significantly inhibited by the combination treatment (Figure 5D). The histological staining showed that lung and liver metastasis were significantly inhibited by combination treatment (Figures S5 and S6). Ultimately, the survival of 4T1-bearing mice in the different treatment groups was monitored, revealing that the combination of CA4-NPs + hs-IMQ significantly extended the overall

DOI: 10.1021/acs.nanolett.9b03214
Nano Lett. 2019, 19, 8021−8031

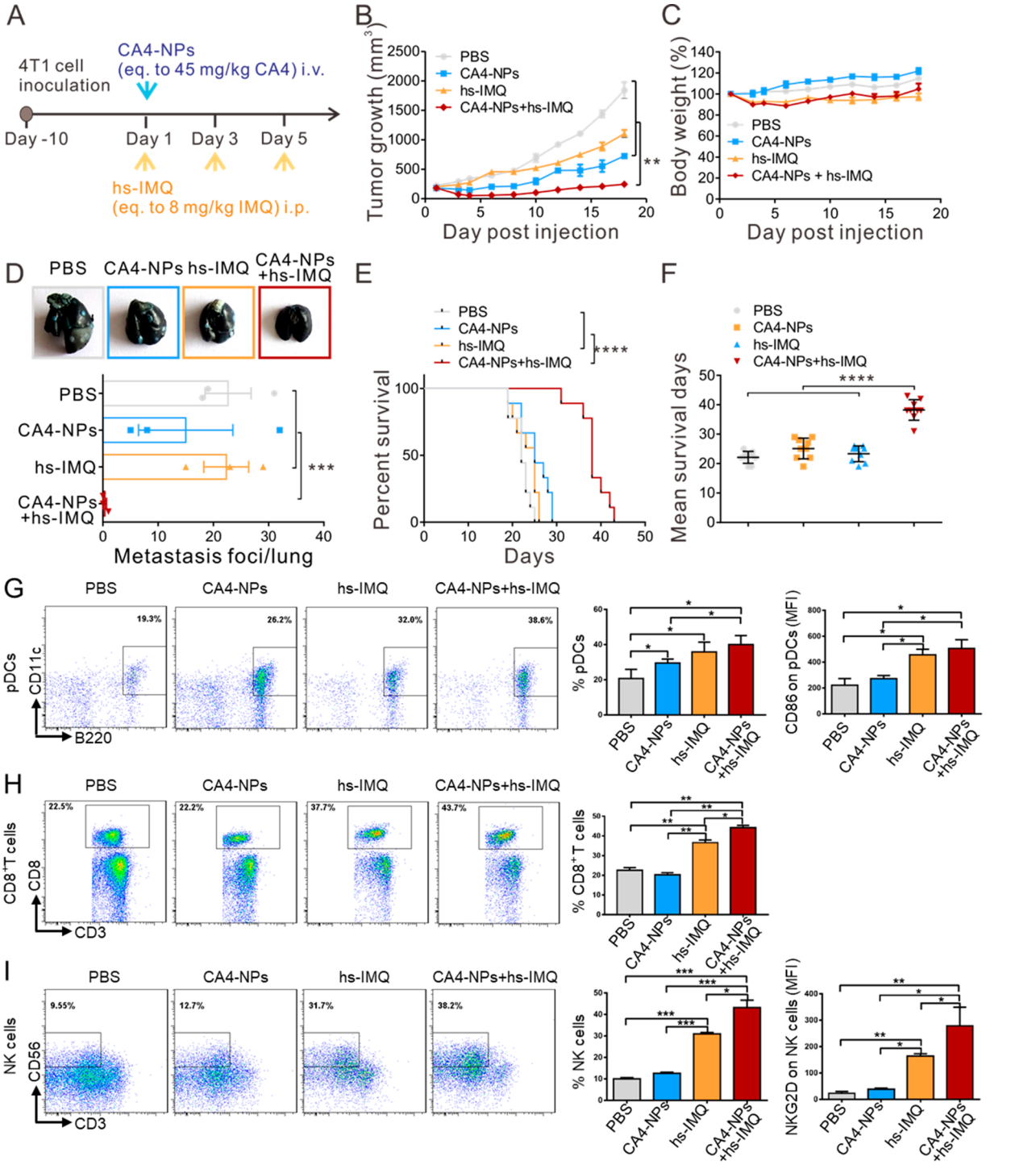

Figure 5. 4T1-bearing Balb/c mice were injected with 45 mg/kg CA4-NPs (equiv to CA4) intravenously on day 1 and/or with 8 mg/kg hs-IMQ (eq to IMQ) intraperitoneally on days 1, 3, and 5. (A) Schematic of the drug treatment. (B, C) Tumor growth curves (B, n = 6 mice/group) and body weight changes (C, n = 6 mice/group) after drug injection. (D) Representative images and quantification of lung metastasis nodules with positive India ink staining (n = 3 mice/group). (E, F) Survival curves (E, n = 9 mice/group) and mean survival days (F, n = 9 mice/group) upon drug treatment. (G–I) Infiltration of pDCs/CD3$^-$CD19$^-$ cells and CD86 on pDCs (G), CTLs/CD45$^+$ cells (H), NK cells/CD45$^+$ cells and NKG2D on NK cells (I) in the tumor microenvironment was determined by flow cytometry at 5 days after administration (n = 3 mice/group). The levels of the indicated activation markers were expressed as the mean fluorescence intensity (MFI), which represented the expression of the activation marker on each subset. In panels B and D–I, data shown are expressed as mean ± SEM. A paired t test was used for statistical comparisons (*p < 0.05, **p < 0.01, ***p < 0.001, ****p < 0.0001).

survival and increased the mean survival of mice compared to all other groups (Figure 5E,F).

Next, the *in vivo* host immunological response to CA4-NPs and hs-IMQ cotreatment in 4T1 tumors (initial tumor volume = 200 mm^3) were studied. Analysis of the tumors 5 days post-treatment showed that the percentage of infiltrated pDCs increased significantly, while the signal intensity of active molecules (CD86) on pDCs in whole tumors of the CA4-NPs

DOI: 10.1021/acs.nanolett.9b03214
Nano Lett. 2019, 19, 8021–8031

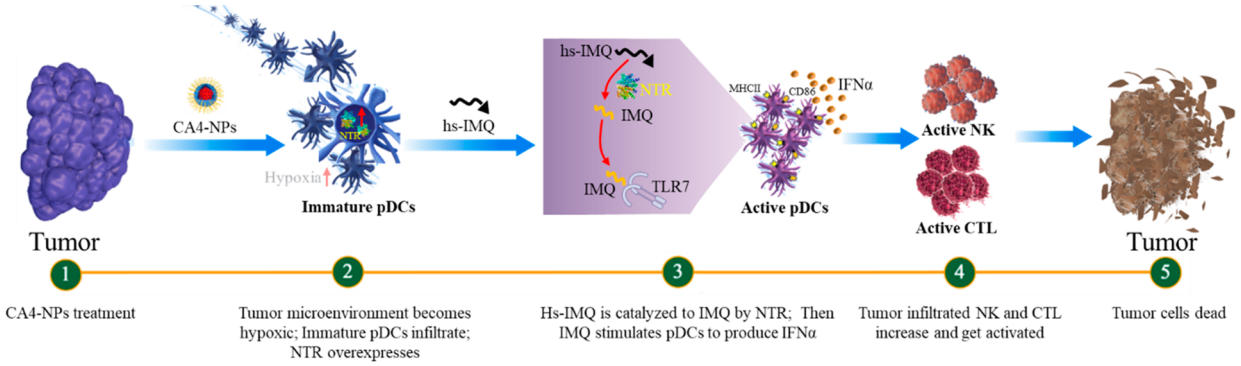

Figure 6. Schematic showing the activation of tumor immunity upon CA4-NPs and hs-IMQ treatment.

group were similar to those of the PBS group, confirming that CA4-NPs could induce immature pDC infiltration into treated tumors. As hs-IMQ can recruit pDCs, the CA4-NPs + hs-IMQ group led to the highest number of pDCs in all groups (Figure 5G, left panel). CD86 expression on pDCs in both the hs-IMQ and CA4-NPs + hs-IMQ groups were significantly higher than other groups, particularly for combination treatment, as hs-IMQ converted the infiltrated immature pDCs into active pDCs (Figure 5G, right panel). The percentage of infiltrated NK, the signal intensity of active molecules (NKG2D) on NK and percentage of infiltrated CTL ($CD8^+$ T cells) did not increase in the CA4-NPs group, relative to the PBS group. Upon hs-IMQ treatment, the percentage of infiltrated NK, the signal intensity of active molecules (NKG2D) on NK and percentage of infiltrated CTL increased significantly, which means NK cells and CTLs were primed and infiltrated the tumors after hs-IMQ treatment. Further, the CA4-NPs + hs-IMQ group had a significantly higher percentage of infiltrated NK, the signal intensity of active molecules (NKG2D) on NK and percentage of infiltrated CTL, compared to hs-IMQ group. Together, CA4-NPs made immature pDCs infiltrated to tumors, and combining with hs-IMQ, the immature pDCs became active and NK cells and CTLs were primed and robustly infiltrated the tumors (Figure 5H and I). Tumor immunity was therefore activated, including natural and adaptive immunity as a result of CA4-NPs + hs-IMQ treatment.

These results clearly demonstrated that CA4-NPs have a synergistic effect with hs-IMQ through a series of processes including the activation of tumor immunity (Figure 6). This can be summarized as follows: (1) following CA4-NPs treatment, (2) the tumors become hypoxic, leading to NTR overexpression and the infiltration of immature pDCs to establish an immunosuppressive microenvironment. (3) When hs-IMQ is converted into IMQ by NTR, (4) pDCs are recruited and activated and produce IFNα, which recruits and activates NK cells and CTLs to create an immune-activated tumor microenvironment. (5) These processes lead to effective tumor cell killing via necrosis and apoptosis, ultimately inhibiting tumor growth and metastasis.

The identification of immature pDC infiltration following CA4-NPs treatment clarifies the mechanisms underlying the repopulation process. Immature pDC infiltration is a side effect of the host immunological response to CA4-NPs treatment, while hs-IMQ selectively activates CA4-NPs-induced hypoxic tumors, enhancing antitumor efficacy. From another aspect, CA4-NPs can serve as tools to recruit intratumoral pDCs, achieving pDC-targeted antitumor therapy. Exploiting these side effects, particularly for pDCs, can enhance therapeutic efficacy given the critical role of pDCs in bridging the natural and adaptive immune systems.

In conclusion, this is the first demonstration of immature pDC recruitment to tumors following VDA treatment. The newly synthesized hs-IMQ activates pDCs to induce IFNα, IL-6, and IL-12p70 secretion, along with infiltration and activation of NK cells and CTLs. The combination of CA4-NPs and hs-IMQ activated both natural and adaptive immune responses conferred by the hypoxia sensitivity of hs-IMQ and the tumor-selective hypoxia induced by CA4-NPs treatment. This resulted in enhanced antitumor effects and metastasis inhibition *in vivo*. This innovative synergistic combination of CA4-NPs and hs-IMQ therefore represents a new paradigm for the modulation of host immunological responses. This potent approach provides further insight for clinical research, expands our understanding of the VDA-related immune side effects, and offers an alternative dosing regimen for IMQ.

■ ASSOCIATED CONTENT

Supporting Information

The Supporting Information is available free of charge on the ACS Publications website at DOI: 10.1021/acs.nanolett.9b03214.

Detailed experimental materials and methods, additional results of preparation and characterization of CA4-NPs and hs-IMQ, evaluation of CXCL12 level after CA4-NPs treatment, figures showing CXCL12 level detection, NMR spectra, and H&E staining (PDF)

■ AUTHOR INFORMATION

Corresponding Authors

*Jingtao Chen. Email: jtchen@jlu.edu.cn.
*Zhaohui Tang. Email: ztang@ciac.ac.cn
*Xuesi Chen. Email: xschen@ciac.ac.cn

ORCID

Na Shen: 0000-0003-1557-1060
Shengcai Yang: 0000-0003-1007-8816
Xuesi Chen: 0000-0003-3542-9256

Author Contributions

#These authors contributed equally.

Author Contributions

All authors have given approval to the final version of the manuscript.

Notes

The authors declare no competing financial interest.

DOI: 10.1021/acs.nanolett.9b03214
Nano Lett. 2019, 19, 8021−8031

■ ACKNOWLEDGMENTS

This work was financially supported by National Natural Science Foundation of China (Projects 51503202, 51673189, 51873206, 51833010, 51520105004, and 81870152), Ministry of Science and Technology of China (2018ZX09711003-012), and Jilin Province (20190103033JH and 20180101097JC).

■ ABBREVIATIONS

VDAs, vascular disrupting agents; CA4-NPs, poly(L-glutamic acid)-*graft*-methoxy poly(ethylene glycol)/combretastatin A4; pDCs, plasmacytoid dendritic cells; hs-IMQ, hypoxia-sensitive imiquimod; IMQ, imiquimod; NTR, nitroreductase; CA4P, combretastatin A4 phosphate; PLG-CA4, combretastatin A4-based nanodrug; NK, natural killer cells; mDCs, myeloid dendritic cells; CTLs, $CD8^+$ T cells; MΦ, macrophages

■ REFERENCES

(1) Schreiber, R. D.; Old, L. J.; Smyth, M. J. Cancer immunoediting: integrating immunity's roles in cancer suppression and promotion. *Science* **2011**, *331*, 1565−70.

(2) Rosenthal, R.; Cadieux, E. L.; Salgado, R.; Bakir, M. A.; Moore, D. A.; Hiley, C. T.; Lund, T.; Tanic, M.; Reading, J. L.; Joshi, K.; Henry, J. Y.; Ghorani, E.; Wilson, G. A.; Birkbak, N. J.; Jamal-Hanjani, M.; Veeriah, S.; Szallasi, Z.; Loi, S.; Hellmann, M. D.; Feber, A.; Chain, B.; Herrero, J.; Quezada, S. A.; Demeulemeester, J.; Van Loo, P.; Beck, S.; McGranahan, N.; Swanton, C.; consortium, T. R. Neoantigen-directed immune escape in lung cancer evolution. *Nature* **2019**, *567*, 479−485.

(3) O'Sullivan, D.; Sanin, D. E.; Pearce, E. J.; Pearce, E. L. Metabolic interventions in the immune response to cancer. *Nat. Rev. Immunol.* **2019**, *19*, 324−335.

(4) Fridman, W. H.; Pages, F.; Sautes-Fridman, C.; Galon, J. The immune contexture in human tumours: impact on clinical outcome. *Nat. Rev. Cancer* **2012**, *12*, 298−306.

(5) Shaked, Y. Balancing efficacy of and host immune responses to cancer therapy: the yin and yang effects. *Nat. Rev. Clin. Oncol.* **2016**, *13*, 611−626.

(6) Ziklo, N.; Huston, W. M.; Taing, K.; Timms, P. High expression of IDO1 and TGF-beta1 during recurrence and post infection clearance with Chlamydia trachomatis, are independent of host IFN-gamma response. *BMC Infect. Dis.* **2019**, *19*, 218.

(7) Aziz, M. H.; Sideras, K.; Aziz, N. A.; Mauff, K.; Haen, R.; Roos, D.; Saida, L.; Suker, M.; van der Harst, E.; Mieog, J. S.; Bonsing, B. A.; Klaver, Y.; Koerkamp, B. G.; van Eijck, C. H. The Systemic-immune-inflammation Index Independently Predicts Survival and Recurrence in Resectable Pancreatic Cancer and its Prognostic Value Depends on Bilirubin Levels: A Retrospective Multicenter Cohort Study. *Ann. Surg.* **2019**, *270*, 139−146.

(8) Clark, W. H., Jr.; Elder, D. E.; Guerry, D. t.; Braitman, L. E.; Trock, B. J.; Schultz, D.; Synnestvedt, M.; Halpern, A. C. Model predicting survival in stage I melanoma based on tumor progression. *J. Natl. Cancer Inst.* **1989**, *81*, 1893−904.

(9) Sato, E.; Olson, S. H.; Ahn, J.; Bundy, B.; Nishikawa, H.; Qian, F.; Jungbluth, A. A.; Frosina, D.; Gnjatic, S.; Ambrosone, C.; Kepner, J.; Odunsi, T.; Ritter, G.; Lele, S.; Chen, Y. T.; Ohtani, H.; Old, L. J.; Odunsi, K. Intraepithelial CD8+ tumor-infiltrating lymphocytes and a high CD8+/regulatory T cell ratio are associated with favorable prognosis in ovarian cancer. *Proc. Natl. Acad. Sci. U. S. A.* **2005**, *102*, 18538−43.

(10) Pages, F.; Berger, A.; Camus, M.; Sanchez-Cabo, F.; Costes, A.; Molidor, R.; Mlecnik, B.; Kirilovsky, A.; Nilsson, M.; Damotte, D.; Meatchi, T.; Bruneval, P.; Cugnenc, P. H.; Trajanoski, Z.; Fridman, W. H.; Galon, J. Effector memory T cells, early metastasis, and survival in colorectal cancer. *N. Engl. J. Med.* **2005**, *353*, 2654−66.

(11) Galon, J.; Costes, A.; Sanchez-Cabo, F.; Kirilovsky, A.; Mlecnik, B.; Lagorce-Pages, C.; Tosolini, M.; Camus, M.; Berger, A.; Wind, P.; Zinzindohoue, F.; Bruneval, P.; Cugnenc, P. H.; Trajanoski, Z.; Fridman, W. H.; Pages, F. Type, density, and location of immune cells within human colorectal tumors predict clinical outcome. *Science* **2006**, *313*, 1960−4.

(12) Hanahan, D.; Coussens, L. M. Accessories to the Crime: Functions of Cells Recruited to the Tumor Microenvironment. *Cancer Cell* **2012**, *21*, 309−322.

(13) Eckstein, N.; Servan, K.; Hildebrandt, B.; Politz, A.; von Jonquieres, G.; Wolf-Kummeth, S.; Napierski, I.; Hamacher, A.; Kassack, M. U.; Budczies, J.; Beier, M.; Dietel, M.; Royer-Pokora, B.; Denkert, C.; Royer, H. D. Hyperactivation of the insulin-like growth factor receptor I signaling pathway is an essential event for cisplatin resistance of ovarian cancer cells. *Cancer Res.* **2009**, *69*, 2996−3003.

(14) Williams, R. T.; den Besten, W.; Sherr, C. J. Cytokine-dependent imatinib resistance in mouse BCR-ABL+, Arf-null lymphoblastic leukemia. *Genes Dev.* **2007**, *21*, 2283−7.

(15) Voloshin, T.; Voest, E. E.; Shaked, Y. The host immunological response to cancer therapy: An emerging concept in tumor biology. *Exp. Cell Res.* **2013**, *319*, 1687−95.

(16) Karagiannis, G. S.; Pastoriza, J. M.; Wang, Y.; Harney, A. S.; Entenberg, D.; Pignatelli, J.; Sharma, V. P.; Xue, E. A.; Cheng, E.; D'Alfonso, T. M.; Jones, J. G.; Anampa, J.; Rohan, T. E.; Sparano, J. A.; Condeelis, J. S.; Oktay, M. H. Neoadjuvant chemotherapy induces breast cancer metastasis through a TMEM-mediated mechanism. *Sci. Transl. Med.* **2017**, *9*, eaan0026.

(17) Chang, Y. S.; Jalgaonkar, S. P.; Middleton, J. D.; Hai, T. Stress-inducible gene Atf3 in the noncancer host cells contributes to chemotherapy-exacerbated breast cancer metastasis. *Proc. Natl. Acad. Sci. U. S. A.* **2017**, *114*, E7159−E7168.

(18) Keklikoglou, I.; Cianciaruso, C.; Guc, E.; Squadrito, M. L.; Spring, L. M.; Tazzyman, S.; Lambein, L.; Poissonnier, A.; Ferraro, G. B.; Baer, C.; Cassara, A.; Guichard, A.; Iruela-Arispe, M. L.; Lewis, C. E.; Coussens, L. M.; Bardia, A.; Jain, R. K.; Pollard, J. W.; De Palma, M. Chemotherapy elicits pro-metastatic extracellular vesicles in breast cancer models. *Nat. Cell Biol.* **2019**, *21*, 190−202.

(19) Ribas, A.; Hamid, O.; Daud, A.; Hodi, F. S.; Wolchok, J. D.; Kefford, R.; Joshua, A. M.; Patnaik, A.; Hwu, W.-J.; Weber, J. S.; Gangadhar, T. C.; Hersey, P.; Dronca, R.; Joseph, R. W.; Zarour, H.; Chmielowski, B.; Lawrence, D. P.; Algazi, A.; Rizvi, N. A.; Hoffner, B.; Mateus, C.; Gergich, K.; Lindia, J. A.; Giannotti, M.; Li, X. N.; Ebbinghaus, S.; Kang, S. P.; Robert, C. Association of Pembrolizumab With Tumor Response and Survival Among Patients With Advanced Melanoma. *JAMA-J. Am. Med. Assoc.* **2016**, *315*, 1600−1609.

(20) Galluzzi, L.; Buque, A.; Kepp, O.; Zitvogel, L.; Kroemer, G. Immunological Effects of Conventional Chemotherapy and Targeted Anticancer Agents. *Cancer Cell* **2015**, *28*, 690−714.

(21) Wang, H.; Tang, Y.; Fang, Y.; Zhang, M.; Wang, H.; He, Z.; Wang, B.; Xu, Q.; Huang, Y. Reprogramming Tumor Immune Microenvironment (TIME) and Metabolism via Biomimetic Targeting Codelivery of Shikonin/JQ1. *Nano Lett.* **2019**, *19*, 2935−2944.

(22) Min, H.; Wang, J.; Qi, Y.; Zhang, Y.; Han, X.; Xu, Y.; Xu, J.; Li, Y.; Chen, L.; Cheng, K.; Liu, G.; Yang, N.; Li, Y.; Nie, G. Biomimetic Metal-Organic Framework Nanoparticles for Cooperative Combination of Antiangiogenesis and Photodynamic Therapy for Enhanced Efficacy. *Adv. Mater.* **2019**, *31*, e1808200.

(23) Oh, D.-Y.; Kim, T.-M.; Han, S.-W.; Shin, D.-Y.; Lee, Y. G.; Lee, K.-W.; Kim, J. H.; Kim, T.-Y.; Jang, I.-J.; Lee, J.-S.; Bang, Y.-J. Phase I Study of CKD-516, a Novel Vascular Disrupting Agent, in Patients with Advanced Solid Tumors. *Cancer Res. and Treat.* **2016**, *48*, 28−36.

(24) Monk, B. J.; Sill, M. W.; Walker, J. L.; Darus, C. J.; Sutton, G.; Tewari, K. S.; Martin, L. P.; Schilder, J. M.; Coleman, R. L.; Balkissoon, J.; Aghajanian, C. Randomized Phase II Evaluation of Bevacizumab Versus Bevacizumab Plus Fosbretabulin in Recurrent Ovarian, Tubal, or Peritoneal Carcinoma: An NRG Oncology/Gynecologic Oncology Group Study. *J. Clin. Oncol.* **2016**, *34*, 2279−2286.

(25) Horsman, M. R.; Siemann, D. W. Pathophysiologic effects of vascular-targeting agents and the implications for combination with conventional therapies. *Cancer Res.* **2006**, *66*, 11520−39.

DOI: 10.1021/acs.nanolett.9b03214
Nano Lett. 2019, 19, 8021−8031

(26) Tozer, G. M.; Kanthou, C.; Baguley, B. C. Disrupting tumour blood vessels. *Nat. Rev. Cancer* **2005**, *5*, 423−435.
(27) Siemann, D. W.; Chaplin, D. J.; Horsman, M. R. Vascular-targeting therapies for treatment of malignant disease. *Cancer* **2004**, *100*, 2491−2499.
(28) Kim, J. J.; Tannock, I. F. Repopulation of cancer cells during therapy: an important cause of treatment failure. *Nat. Rev. Cancer* **2005**, *5*, 516−25.
(29) Welford, A. F.; Biziato, D.; Coffelt, S. B.; Nucera, S.; Fisher, M.; Pucci, F.; Di Serio, C.; Naldini, L.; De Palma, M.; Tozer, G. M.; Lewis, C. E. TIE2-expressing macrophages limit the therapeutic efficacy of the vascular-disrupting agent combretastatin A4 phosphate in mice. *J. Clin. Invest.* **2011**, *121*, 1969−1973.
(30) Galbraith, S. M.; Maxwell, R. J.; Lodge, M. A.; Tozer, G. M.; Wilson, J.; Taylor, N. J.; Stirling, J. J.; Sena, L.; Padhani, A. R.; Rustin, G. J. Combretastatin A4 phosphate has tumor antivascular activity in rat and man as demonstrated by dynamic magnetic resonance imaging. *J. Clin. Oncol.* **2003**, *21*, 2831−42.
(31) Shaked, Y.; Tang, T.; Woloszynek, J.; Daenen, L. G.; Man, S.; Xu, P.; Cai, S.-R.; Arbeit, J. M.; Voest, E. E.; Chaplin, D. J.; Smythe, J.; Harris, A.; Nathan, P.; Judson, I.; Rustin, G.; Bertolini, F.; Link, D. C.; Kerbel, R. S. Contribution of Granulocyte Colony-Stimulating Factor to the Acute Mobilization of Endothelial Precursor Cells by Vascular Disrupting Agents. *Cancer Res.* **2009**, *69*, 7524−7528.
(32) Liu, T.; Zhang, D.; Song, W.; Tang, Z.; Zhu, J.; Ma, Z.; Wang, X.; Chen, X.; Tong, T. A poly(l-glutamic acid)-combretastatin A4 conjugate for solid tumor therapy: Markedly improved therapeutic efficiency through its low tissue penetration in solid tumor. *Acta Biomater.* **2017**, *53*, 179−189.
(33) Swiecki, M.; Colonna, M. The multifaceted biology of plasmacytoid dendritic cells. *Nat. Rev. Immunol.* **2015**, *15*, 471−85.
(34) Ceradini, D. J.; Kulkarni, A. R.; Callaghan, M. J.; Tepper, O. M.; Bastidas, N.; Kleinman, M. E.; Capla, J. M.; Galiano, R. D.; Levine, J. P.; Gurtner, G. C. Progenitor cell trafficking is regulated by hypoxic gradients through HIF-1 induction of SDF-1. *Nat. Med.* **2004**, *10*, 858−64.
(35) Shaked, Y.; Tang, T.; Woloszynek, J.; Daenen, L. G.; Man, S.; Xu, P.; Cai, S. R.; Arbeit, J. M.; Voest, E. E.; Chaplin, D. J.; Smythe, J.; Harris, A.; Nathan, P.; Judson, I.; Rustin, G.; Bertolini, F.; Link, D. C.; Kerbel, R. S. Contribution of granulocyte colony-stimulating factor to the acute mobilization of endothelial precursor cells by vascular disrupting agents. *Cancer Res.* **2009**, *69*, 7524−8.
(36) Welford, A. F.; Biziato, D.; Coffelt, S. B.; Nucera, S.; Fisher, M.; Pucci, F.; Di Serio, C.; Naldini, L.; De Palma, M.; Tozer, G. M.; Lewis, C. E. TIE2-expressing macrophages limit the therapeutic efficacy of the vascular-disrupting agent combretastatin A4 phosphate in mice. *J. Clin. Invest.* **2011**, *121*, 1969−73.
(37) Wei, S.; Kryczek, I.; Zou, L.; Daniel, B.; Cheng, P.; Mottram, P.; Curiel, T.; Lange, A.; Zou, W. Plasmacytoid dendritic cells induce CD8+ regulatory T cells in human ovarian carcinoma. *Cancer Res.* **2005**, *65*, 5020−6.
(38) Michea, P.; Noël, F.; Zakine, E.; Czerwinska, U.; Sirven, P.; Abouzid, O.; Goudot, C.; Scholer-Dahirel, A.; Vincent-Salomon, A.; Reyal, F.; Amigorena, S.; Guillot-Delost, M.; Segura, E.; Soumelis, V. Adjustment of dendritic cells to the breast-cancer microenvironment is subset specific. *Nat. Immunol.* **2018**, *19*, 885−897.
(39) Oberkampf, M.; Guillerey, C.; Mouriès, J.; Rosenbaum, P.; Fayolle, C.; Bobard, A.; Savina, A.; Ogier-Denis, E.; Enninga, J.; Amigorena, S.; Leclerc, C.; Dadaglio, G. Mitochondrial reactive oxygen species regulate the induction of CD8+ T cells by plasmacytoid dendritic cells. *Nat. Commun.* **2018**, *9*, 2241.
(40) Conrad, C.; Gregorio, J.; Wang, Y.-H.; Ito, T.; Meller, S.; Hanabuchi, S.; Anderson, S.; Atkinson, N.; Ramirez, P. T.; Liu, Y.-J.; Freedman, R.; Gilliet, M. Plasmacytoid Dendritic Cells Promote Immunosuppression in Ovarian Cancer via ICOS Costimulation of Foxp3(+) T-Regulatory Cells. *Cancer Res.* **2012**, *72*, 5240−5249.
(41) Tang, Q.; Bluestone, J. A. Plasmacytoid DCs and T(reg) cells: casual acquaintance or monogamous relationship? *Nat. Immunol.* **2006**, *7*, 551−3.
(42) Capone, I.; Marchetti, P.; Ascierto, P. A.; Malorni, W.; Gabriele, L. Sexual Dimorphism of Immune Responses: A New Perspective in Cancer Immunotherapy. *Front. Immunol.* **2018**, *9*, 552.
(43) Irla, M.; Kupfer, N.; Suter, T.; Lissilaa, R.; Benkhoucha, M.; Skupsky, J.; Lalive, P. H.; Fontana, A.; Reith, W.; Hugues, S. MHC class II-restricted antigen presentation by plasmacytoid dendritic cells inhibits T cell-mediated autoimmunity. *J. Exp. Med.* **2010**, *207*, 1891−905.
(44) Hellman, P.; Eriksson, H. Early activation markers of human peripheral dendritic cells. *Hum. Immunol.* **2007**, *68*, 324−33.
(45) Hanabuchi, S.; Watanabe, N.; Wang, Y. H.; Wang, Y. H.; Ito, T.; Shaw, J.; Cao, W.; Qin, F. X.; Liu, Y. J. Human plasmacytoid predendritic cells activate NK cells through glucocorticoid-induced tumor necrosis factor receptor-ligand (GITRL). *Blood* **2006**, *107*, 3617−23.
(46) Wang, R.; Zhang, J.-L.; Wei, B.; Tian, Y.; Li, Z.-H.; Wang, L.; Du, C. Upregulation of plasmacytoid dendritic cells in glioma. *Tumor Biol.* **2014**, *35*, 9661−9666.
(47) Drobits, B.; Holcmann, M.; Amberg, N.; Swiecki, M.; Grundtner, R.; Hammer, M.; Colonna, M.; Sibilia, M. Imiquimod clears tumors in mice independent of adaptive immunity by converting pDCs into tumor-killing effector cells. *J. Clin. Invest.* **2012**, *122*, 575−85.
(48) Kalb, M. L.; Glaser, A.; Stary, G.; Koszik, F.; Stingl, G. TRAIL (+) human plasmacytoid dendritic cells kill tumor cells in vitro: mechanisms of imiquimod- and IFN-alpha-mediated antitumor reactivity. *J. Immunol.* **2012**, *188*, 1583−91.
(49) Aspord, C.; Tramcourt, L.; Leloup, C.; Molens, J. P.; Leccia, M. T.; Charles, J.; Plumas, J. Imiquimod Inhibits Melanoma Development by Promoting pDC Cytotoxic Functions and Impeding Tumor Vascularization. *J. Invest. Dermatol.* **2014**, *134*, 2551−2561.
(50) Holcmann, M.; Drobits, B.; Sibilia, M. How imiquimod licenses plasmacytoid dendritic cells to kill tumors. *Oncoimmunology* **2012**, *1*, 1661−1663.
(51) Soong, R.-S.; Song, L.; Trieu, J.; Knoff, J.; He, L.; Tsai, Y.-C.; Huh, W.; Chang, Y.-N.; Cheng, W.-F.; Roden, R. B. S.; Wu, T. C.; Trimble, C. L.; Hung, C.-F. Toll-like Receptor Agonist Imiquimod Facilitates Antigen-Specific CD8(+) T-cell Accumulation in the Genital Tract Leading to Tumor Control through IFN gamma. *Clin. Cancer Res.* **2014**, *20*, 5456−5467.
(52) Savage, P.; Horton, V.; Moore, J.; Owens, M.; Witt, P.; Gore, M. E. A phase I clinical trial of imiquimod, an oral interferon inducer, administered daily. *Br. J. Cancer* **1996**, *74*, 1482−1486.
(53) Hanger, C.; Dalrymple, J.; Hepburn, D. Systemic side effects from topical imiquimod. *N. Z. Med. J.* **2005**, *118*, U1682.
(54) Goldstein, D.; Hertzog, P.; Tomkinson, E.; Couldwell, D.; McCarville, S.; Parrish, S.; Cunningham, P.; Newell, M.; Owens, M.; Cooper, D. A. Administration of imiquimod, an interferon inducer, in asymptomatic human immunodeficiency virus-infected persons to determine safety and biologic response modification. *J. Infect. Dis.* **1998**, *178*, 858−61.
(55) Yang, S.; Tang, Z.; Hu, C.; Zhang, D.; Shen, N.; Yu, H.; Chen, X. Selectively Potentiating Hypoxia Levels by Combretastatin A4 Nanomedicine: Toward Highly Enhanced Hypoxia-Activated Prodrug Tirapazamine Therapy for Metastatic Tumors. *Adv. Mater.* **2019**, *31*, 1805955.
(56) Landowski, T. H.; Guntle, G. P.; Zhao, D.; Jagadish, B.; Mash, E. A.; Dorr, R. T.; Raghunand, N. Magnetic Resonance Imaging Identifies Differential Response to Pro-Oxidant Chemotherapy in a Xenograft Model. *Transl. Oncol.* **2016**, *9*, 228−235.
(57) Robinson, S. P.; Griffiths, J. R. Current issues in the utility of F-19 nuclear magnetic resonance methodologies for the assessment of tumour hypoxia. *Philos. Trans. R. Soc., B* **2004**, *359*, 987−996.
(58) Uddin, M. I.; Evans, S. M.; Craft, J. R.; Marnet, L. J.; Uddin, M. J.; Jayagopal, A. Applications of Azo-Based Probes for Imaging Retinal Hypoxia. *ACS Med. Chem. Lett.* **2015**, *6*, 445−449.
(59) Brown, J. M.; William, W. R. Exploiting tumour hypoxia in cancer treatment. *Nat. Rev. Cancer* **2004**, *4*, 437−447.

DOI: 10.1021/acs.nanolett.9b03214
Nano Lett. 2019, 19, 8021−8031

(60) Liu, Z.-R.; Tang, Y.; Xu, A.; Lin, W. A new fluorescent probe with a large turn-on signal for imaging nitroreductase in tumor cells and tissues by two-photon microscopy. *Biosens. Bioelectron.* **2017**, *89*, 853−858.

DOI: 10.1021/acs.nanolett.9b03214
Nano Lett. 2019, 19, 8021−8031